(Received 14 May 2025, Accepted 23 June 2025, Scheduled 11 July 2025)

A Compact Parasitic Mushroom Patch Loaded Antenna for 5G MM-Wave Applications (28 GHz/38 GHz)

Tarik El-Arrouch[1], Abdelaaziz El Ansari[1,*], Najiba El Amrani El Idrissi[1], Mahadu A. Trimukhe[2], Shobhit Khandare[3], Zahriladha Zakaria[4], and Ahmed J. A. Al-Gburi[4,*]

[1] *Signals, Systems and Components Laboratory, Faculty of Science and Technology Sidi Mohammed Ben Abdellah University, Fez, Morocco*
[2] *Bharati Vidyapeeth (Deemed to be University), Navi Mumbai, India*
[3] *Vivekanand Education Society's Institute of Technology (VESIT), Mumbai, India*
[4] *Center for Telecommunication Research & Innovation (CeTRI) Fakulti Teknologi Dan Kejuruteraan Elektronik Dan Komputer (FTKEK) Universiti Teknikal Malaysia Melaka (UTeM), Jalan Hang Tuah Jaya, Durian Tunggal 76100, Malaysia*

ABSTRACT: This study introduces and evaluates a smaller rectangular antenna featuring parasitic mushroom patches to achieve enhanced gain and wide impedance bandwidth (WIBW) for 5G millimeter-wave (mm-wave) applications (28 GHz/38 GHz). The antenna structure consists of a simple rectangular patch fed by an inset feed microstrip line operating at 50 Ω. To improve the antenna gain and impedance bandwidth, a parasitic mushroom structure is introduced around the edges of the main patch. Additionally, to further enhance operating bandwidth and matching, two rectangular Defected Ground Structures (DGSs) are incorporated in the bottom side. The antenna is fabricated on a low-cost substrate specifically FR4 ($\varepsilon_r = 4.4$, tang$\delta = 0.02$), with dimensions of $(12 \times 13 \times 0.8)\,\text{mm}^3$. The results demonstrate a wide impedance bandwidth of 14.2 GHz (50.71% FBW) covering frequencies of 25.98 GHz to 40.18 GHz, and the antenna achieves a maximum gain of 7.20 dB at 28 GHz and maintains an efficiency more than 80% across the entire bandwidth. These outcomes make the antenna a good choice for 5G applications at 28 GHz and 38 GHz.

1. INTRODUCTION

Today, antennas are designed to meet the requirements of 5G and future 6G applications in terms of high data rates, capacity, connectivity, and low latency. 5G networks operate at millimeter-wave frequencies, typically in the range of 24 GHz–300 GHz, enabling high data rates and low latency. These frequencies, while offering significant bandwidth advantages, also present challenges such as increased propagation losses and susceptibility to environmental obstacles due to the multipath. As such, antennas for 5G applications must be meticulously engineered to deliver high gain, wide bandwidth, and efficient performance across these frequency bands. Patch antennas for 5G and 6G are highly sought after due to them low cost, simplicity in design, and optimization [1–3]. However, traditional patch antennas often suffer from low gain and narrow operating bandwidth limitations [4–6]. Therefore, there is a growing demand for broadband antennas that offer high gain while maintaining a compact size for 5G wireless communication systems. To overcome those limitations, several researches have focused on developing a broadband compact antenna with simple geometry and high gain. The authors in [7] propose a dual-polarized antenna for 5G communication system at 28 GHz, but the antenna with dimensions $(6 \times 8 \times 0.837)\,\text{mm}^3$ suffers from a limited bandwidth of 3.5 GHz and a low gain of 5.89 dBi. A compact wideband antenna for Ka band is proposed in [8], designed using a Roger's substrate. The antenna has good operating bandwidth more than 20 GHz but limited by low gain of 3.87 dB at 28 GHz. In [9], a smaller broadband antenna for mm-wave bands is presented. That structure is constructed on an RT Rogers 3003 substrate and fed using the CPW method. It features a miniature size $(9.25 \times 8.2 \times 0.13)\,\text{mm}^3$ and achieves a good bandwidth of 22 GHz. However, that antenna suffers from a maximum gain of 4.5 dB. In [10], a printed patch $(15 \times 14 \times 0.82)\,\text{mm}^3$ for mm-wave applications is introduced. The antenna is graved on a PET flexible dielectric. In [11], an mm-wave conformal antenna for K and Ka bands is discussed. That antenna covers a super wide bandwidth from 7 GHz to 40 GHz with a peak gain of 5 dB and is designed on a compact FR4 substrate. However, it suffers from a gain of 0.19 dB and a limited bandwidth of 7 GHz. In [12], an oversized patch for 5G mm-wave bands is designed and evaluated. That structure exhibits an excellent gain of 12.6 dB at 28 GHz. However, it suffers from a complex geometry and large size $(25 \times 20 \times 0.157)\,\text{cm}^3$, with a low bandwidth of 6.65 GHz. In [13], the authors present a dual-band compact monopole for multiple-input multiple-output (MIMO) antennas at mm-wave bands. This antenna addresses the limitations in gain and bandwidth of the previously mentioned single antenna. In [14], a compact circular patch is designed for a 5G millimeter wave MIMO structure. Constructed on a Rogers 5880 material with dimensions of $(10 \times 10 \times 1.575)\,\text{cm}^3$, this antenna

* Corresponding authors: Abdelaaziz El Ansari (abdelaaziz.elansari1@usmba.ac.ma); Ahmed J. A. Al-Gburi (ahmedjamal@utem.edu.my).

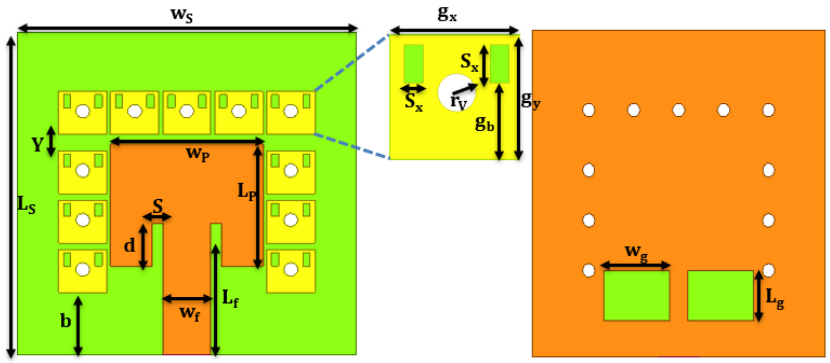

FIGURE 1. Proposed antenna geometry.

is characterized by a narrow bandwidth of 3.52 GHz and maximum gain of 7.1 dB at 28 GHz. In [15], a simple monopole is designed for MIMO applications in mm-wave bands. This antenna, evaluated and realized on a Rogers substrate having overall size of ($12 \times 7 \times 0.203$ cm), shows a limited operating impedance bandwidth of 2.9 GHz and low gain of 4.69 dB at 28 GHz. In [16–21], several compact wideband antennas using different methods are proposed and analyzed for 5G millimeter wave bands. On the other hand, high frequencies, particularly in the millimeter-wave range, are particularly susceptible to attenuation due to phenomena such as multipath transmission and reception. This occurs when an emitted signal follows multiple paths before reaching the receiver, creating interference and variations in the received signal's power [21]. At high frequencies, the propagation of electromagnetic waves is more affected by physical obstacles such as buildings, trees, or even particles in the air, which can cause reflection, diffraction, and scattering. As a result, the signal quality degrades, which can reduce communication capacity. Hence, there is increasing demand for antennas with wide bandwidth and high gain to overcome these challenges, including the use of MIMO technologies [23, 24]. In [25], a double substrate is used to generate a triple band antenna. In [26–28], the authors using slot and stub to improve the antenna bandwidth.

The aims of this paper are to introduce and implement a compact antenna tailored for 5G millimeter-wave bands (28 GHz/38 GHz). The proposed antenna is designed using a miniature FR4 substrate measuring ($12 \times 13 \times 0.8\,\text{mm}^3$). It covers a wide impedance bandwidth of 14.20 GHz, ranging from 25.98 GHz to 40.18 GHz with return losses up to -41.41 dB, and achieves a high gain of 7.20 dB at 28 GHz. Previous antenna structures in [7–12] have utilized high-cost Roger's substrate materials to achieve compact size and broad bandwidth. In contrast, our paper presents a simple and compact wideband antenna for 5G applications using a low-cost FR4 substrate. The antenna's impedance bandwidth is expanded by incorporating a parasitic mushroom patch structure along with Defected Ground Structures (DGSs). Our proposed antenna achieves more than a 75% wider bandwidth than recent literature. the proposed structure is optimized using High Frequency Structure Simulator (HFSS) software. Fabricating the proposed antenna confirms the accuracy of the simulation results.

This work is organized as follows. The process of the antenna designs is outlined in Section 2. The surface current distribution is presented and analyzed in Section 3. Parametric studies are presented in Section 4. Section 5 focuses on the impact of different substrates and the selection of the most suitable substrate. The Results are discussed in Section 6. Section 7 includes a comparative study with other works. Finally, we conclude our work in Section 8.

2. ANTENNA DESIGN

This part presents a detailed study on the structure of the proposed broadband antenna for 5G applications in the mm-wave band. The final geometry of the suggested structure is illustrated in Figure 1. The proposed antenna consists of a simple rectangular main patch (dimensions $W_P = 12$ mm and $L_P = 13$ mm), fed using microstrip line with dimensions of ($W_f = 1.22$ mm, $L_f = 2.23$ mm) and adapted by inset feed ($S = 0.48$ mm, $d = 0.6$ mm). A rectangular mushroom parasitic patch with dimension of ($g_x = 1.4$ mm, $g_Y = 1.3$ mm) is incorporated around the main patch. The patches, feed line, and ground plane are designed using Prefect Electric Conductors (PEC) material with a thickness of $h_P = 0.035$ mm. The antenna is etched on a low-cost FR4 substrate with a dielectric constant of 4.4, a loss tangent of 0.02, and a thickness of 0.8 mm. The antenna structure is analyzed and optimized using the ANSYS HFSS simulator. Proper construction of the antenna feeding is crucial for achieving proper impedance matching. At high signal frequencies, the feeding lines play a vital role in antenna performance. For optimal performance, the impedance of the feeding line should match the characteristic impedance of the patch. In this research, an inset feed approach is employed to ensure proper feeding of the antenna. A microstrip feed line with the characteristic impedance of 50 Ω is used to excite this antenna. The final dimensions of the antenna are $(12 \times 13 \times 0.8)\,\text{mm}^3$. The optimal parameters and dimensions of the proposed antenna are listed in Table 1. Figure 2 depicts the evolutionary stages of our antenna design. Initially, we began with a basic rectangular patch antenna equipped with an inset feed and designed using equations found in the literature [1–6]. This antenna resonates at 28 GHz with a narrow bandwidth of 10.82 GHz and low gain of 4.6 dB (Ant. 1). After iteration two (Ant. 2), we incorporated mushroom-shaped para-

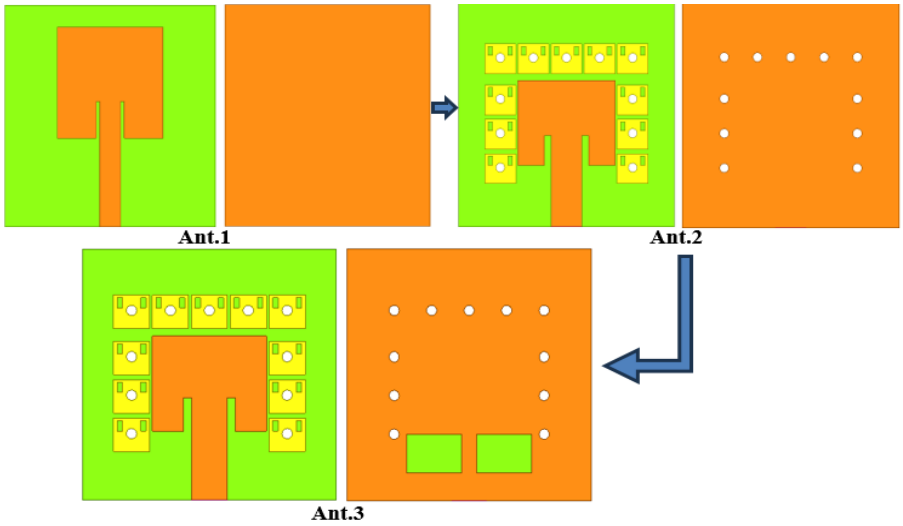

FIGURE 2. Antenna evolution steps.

TABLE 1. Antenna's parameters and optimized dimensions.

Component	Parameters	Value (mm)
substrate	W_S	12
	L_S	13
Patch	W_P	4.5
	L_P	4.5
Feed line	W_f	1.4
	L_f	5
DGS	W_g	2.2
	L_g	1.2
Parasitic mushroom patch	g_X	1.4
	g_Y	1.3
Slot	S_x	0.2
	S_Y	0.4
Via	r_V	0.2

sitic patches around the edges of the main patch to enhance antenna gain. Additionally, this configuration introduced another resonance at a higher frequency. Furthermore, to achieve the wideband characteristics desired for the proposed antenna, two rectangular DGSs were etched into the ground plane (Ant. 3).

The dimensions of rectangular patch, W_p and L_p, are calculated using Equations (1)–(2), where f_r is the resonance frequency ($f_r = 28$ GHz), ε_r a relative permittivity of the substrate, and c the speed of light. The width of microstrip line is calculated from (3), where Z_0 is the characteristic input impedance of the inserted microstrip line. The length of inset feed (d) is calculated by (4), where ε_{eff} is the effective permittivity, given by (5), ΔL the extension of the length calculated from (6), and h_s the substrate thickness [29–33],

$$W_P = \frac{c}{2 \cdot f_r} \cdot \sqrt{\frac{2}{1+\varepsilon_{reff}}} \tag{1}$$

$$L_P = \frac{c}{2 \cdot f_r \cdot \sqrt{\varepsilon_{reff}}} \cdot \ln\left(\frac{8h_S}{w_f} + \frac{w_f}{4h_S}\right) \tag{2}$$

$$Z_0 = \frac{60}{\sqrt{\varepsilon_{reff}}} \cdot \ln\left(\frac{8h_S}{w_f} + \frac{w_f}{4h_S}\right) \tag{3}$$

$$d = \frac{L_P}{2 \cdot \sqrt{\varepsilon_{reff}}} \tag{4}$$

$$\varepsilon_{reff} = \frac{1+\varepsilon_{reff}}{2} + \frac{\varepsilon_{reff-1}}{2} \cdot \sqrt{1+12\frac{w_s}{w_p}} \tag{5}$$

$$\Delta L = 0.412 \cdot h_s \cdot \frac{(0.3+\varepsilon_{reff})\left(\frac{W_P}{h_S}+0.264\right)}{(\varepsilon_{reff}-0.258)\left(\frac{W_P}{h_S}+0.813\right)} \tag{6}$$

These equations are implemented in MATLAB software [34] to compute the parameters of the proposed structure. The obtained values are presented in Table 1.

To demonstrate the steps of the final wideband antenna mechanism, Figure 3 depicts the simulated return loss at various stages of its development. It can be noted that the return losses reach −18 dB with a bandwidth of 1.82 GHz and a modest gain of 4.6 dB for the first Ant. 1 (Step 1). In the second design, Ant. 2 (Step 2), an additional resonance is generated at

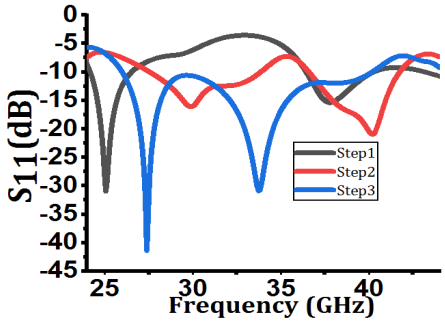

FIGURE 3. Reflection coefficient of different steps.

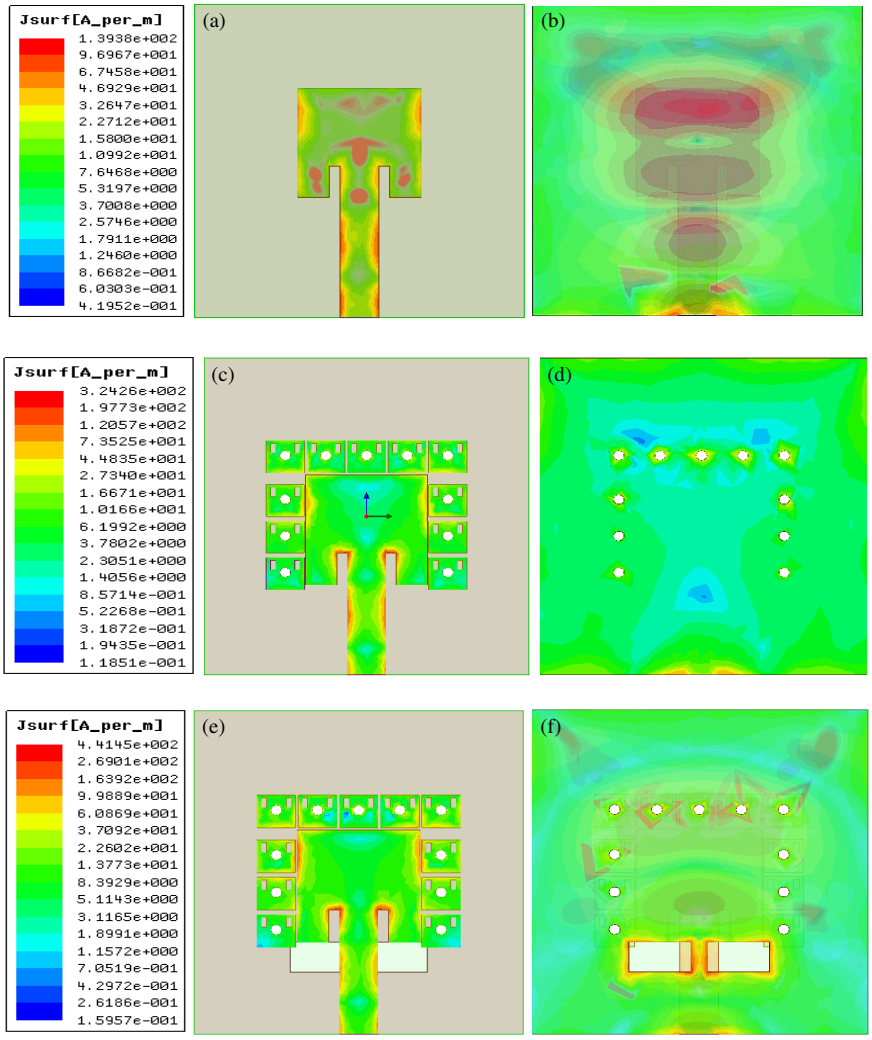

FIGURE 4. Distribution current of different steps: Ant. 1, (a) upper side, (b) lower side, Ant. 2, (c) upper side, (d) lower side, Ant. 3, (e) upper side, (f) lower side.

a higher frequency by incorporating a parasitic mushroom patch around the edges of the main patch, leveraging mutual coupling between the main patch and parasitic patch. This configuration also enhances the antenna gain by 6 dB at 28 GHz. Subsequently, in Ant. 3 (Step 3), the introduction of two rectangular DGSs significantly enhances all performance metrics. The gain is increased to 7.5 dB; the bandwidth expands to 14.20 GHz; and the reflection coefficient is reduced to -42 dB at 28 GHz.

3. CURRENT DISTRIBUTION

To understand the mechanism behind the different stages of the design, Figures 4(a), (b), (c), (d), (e), and (f) illustrate the surface current distributions on the upper and lower sides of the proposed antenna at 28 GHz. In Step 1, the surface current is predominantly distributed along the feedline and the edges of the patch, as shown in Figures 4(a) and (b). On the other hand, as depicted in Figure 3, antenna (Ant. 1) resonates at 25 GHz with a very narrow bandwidth of 1.82 GHz. However, when the parasitic mushroom elements are introduced around the main radiating patch, the surface current is significantly enhanced along the feedline and at the edges of the parasitic patch as depicted in Figures 4(c) and (d). As a result of these modifications, the antenna generates an additional resonance at a higher frequency (Figure 3), caused by the mutual coupling between the main patch and parasitic elements. Finally to improve the antenna's bandwidth and gain, the ground plane was modified in Step 3 by adding two rectangular DGSs below the feedline. This modification disrupts the current direction on the ground plane, as depicted in Figures 4(e) and (f), resulting in a wide impedance bandwidth ranging from 25.98 GHz to 40.18 GHz as shown Figure 3.

4. PARAMETRIC ANALYSIS

To better understand and analyze the impact of various parameters on the return loss (S_{11}), impedance bandwidth (IBW), and gain of the broadband antenna, a parametric analysis is presented in this part. Specifically, five parameters w_g, L_g, g_x, g_Y, and r_V are investigated using HFSS ANSYS software.

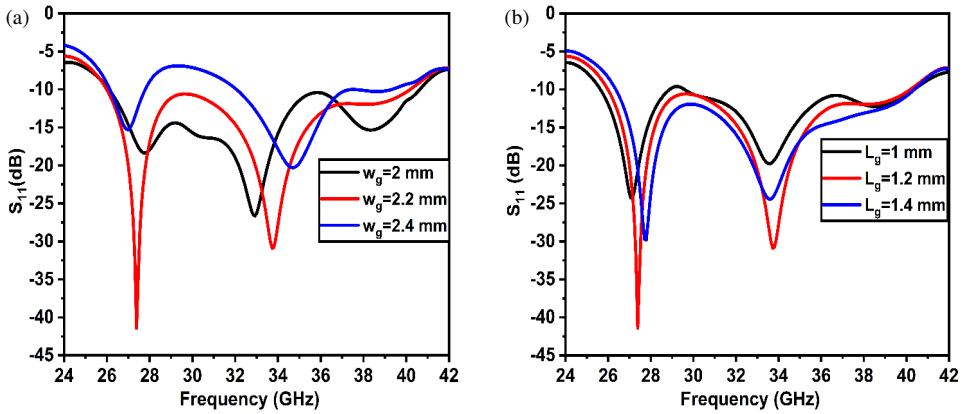

FIGURE 5. Reflection coefficient (a) of various values for w_g, (b) of various values for L_g.

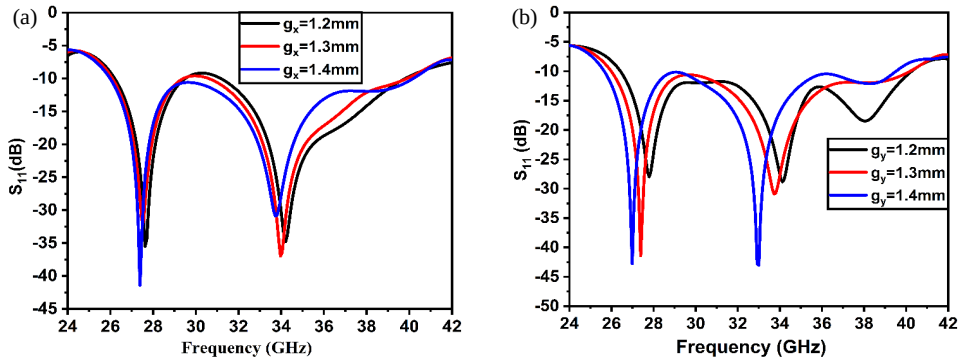

FIGURE 6. Reflection coefficient (a) effect of g_x, (b) effect of g_y.

4.1. The Effects of Width w_g and Length l_g of DGS

The variations of return loss (S_{11}) with different values of w_g and L_g are depicted in Figures 5(a) and (b), respectively. From Figure 5(a), it can be observed that as w_g decreases, the impedance bandwidth improves, and the return loss shifts towards higher frequencies. These findings highlight the significant impact of the width w_g of the DGS on impedance matching and antenna bandwidth. The optimal width w_g that achieves good adaptation at the desired frequency is $w_g = 2$ mm.

The impact of length L_g of the DGS on the S_{11} of the proposed antenna is depicted in Figure 5(b). As shown in this figure, the length L_g significantly affects the impedance bandwidth. It is observed that as L_g decreases from 1.6 mm to 1 mm, the return loss shifts towards lower frequencies, thereby enhancing impedance matching, although there is only a slight change at higher frequencies. The optimal selected value of L_g improves impedance matching and widens the bandwidth, specifically $L_g = 1.2$ mm.

4.2. The Effect of Dimensions of Parasitic Mushroom Patch

The length and width of the parasitic mushroom patch are critical parameters influencing the antenna's bandwidth and gain. The impact of these dimensions on reflection coefficient is illustrated in Figures 6(a) and (b). In Figure 6(a), it is observed that as the width increases, the impedance bandwidth improves, with a slight shift in the resonant frequency towards higher values. The optimal selected width is $g_x = 1.3$ mm to achieve the desired bandwidth. Figure 6(b) illustrates the effect of varying the length of the parasitic patch. It is evident that antenna matching improves as the g_Y value is increased from 1.2 mm to 1.4 mm. Therefore, to achieve optimal performance within the desired impedance band, an appropriate value of g_Y is determined to be 1.4 mm.

4.3. The Effects of Radius r_V of Via

Figure 7 illustrates the variation of S_{11} for different values of the via radius r_V to assess the impact of vias on the antenna's impedance bandwidth. It can be observed that as the via radius r_V increases from 0.1 mm to 0.4 mm, the reflection coefficient S_{11} shifts towards lower frequencies. This shift indicates that larger via radius introduces additional inductive effects, effectively lowering the resonant frequency. The optimal $r_V = 0.2$ mm provides the best impedance matching at the desired frequency.

To analyze the theory behind wideband antennas for 5G applications in the mm-wave band, an equivalent circuit model based on the input impedance response is derived from a full-wave EM solver. The input impedance characteristics indicate that a wideband antenna can be modeled using resonance circuits, which equivalently represent a parallel RLC circuit. The equivalent circuit model, based on this concept for achieving

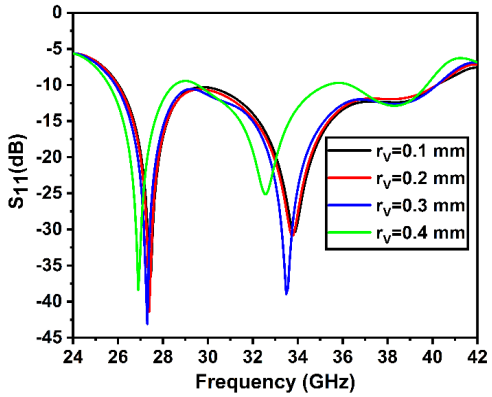

FIGURE 7. Reflection coefficient for different values of radius r_V.

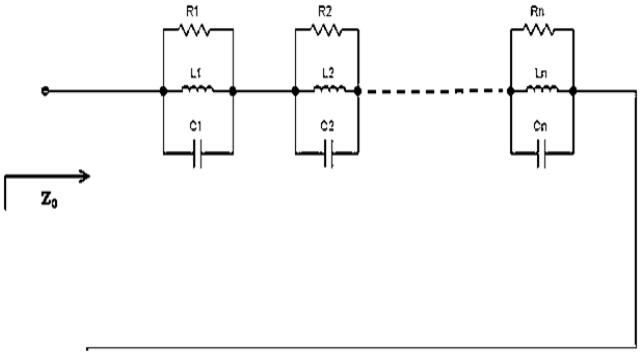

FIGURE 8. Equivalent circuit of the proposed antenna.

wide bandwidth, is depicted in Figure 8.

$$Z_{La} = \sum_{j=1}^{n} \frac{jwRjLj}{Rj\left(1 - w^2LjCj\right) + jwLj} \tag{7}$$

From either simulated or measured results corresponding to resonances (Z_{La}), the values of consecutive parameters in the equivalent circuit model (Rj, Lj, Cj) are calculated using Equation (7). Figure 9 displays the real and imaginary parts of the input impedance of the proposed antenna. It can be observed that the real part varies around 50 Ω, while the imaginary part hovers around zero ohms. The rectangular antenna can be represented by a parallel combination of $R1$, $L1$, and $C1$. The current flowing through vias induces an inductive effect represented by the inductor LLL, while the gaps between adjacent patches introduce a capacitive effect represented by capacitor CCC. By etching rectangular slots on the metallic patch of the Electromagnetic Band Gap (EBG) cell, the series equivalent capacitance can be increased, resulting in a more compact EBG structure and wider bandwidth.

5. IMPACT OF VARIOUS DIELECTRIC SUBSTRATE

To evaluate the impact of different substrates on the antenna's performance in terms of bandwidth and gain, the proposed antenna is investigated with other substrates such as Rogers RT5880, Polyimide, and polyamide. The specifications of the various materials in terms of dielectric constant and loss tangent are summarized in Table 2.

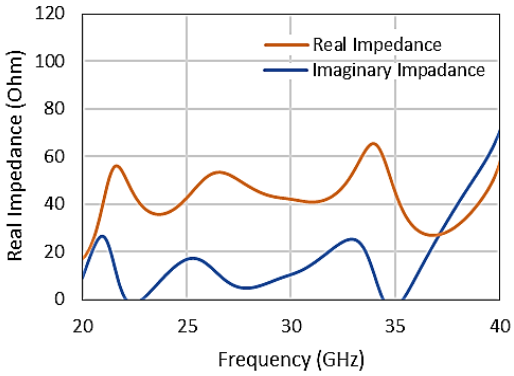

FIGURE 9. Impedance of the proposed antenna.

TABLE 2. Specification dielectric of various substrates.

Substrate	Dielectric constant	Loss tangent
FR-4	4.4	0.02
Polyamide	4.3	0.004
Polyimide	3.5	0.008
Rogers 5880	2.2	0.0009

Figures 10(a) and (b) illustrate the variations in S_{11} and gain, respectively, for different substrates. It can be observed that the proposed antenna with FR-4 provides a wider impedance bandwidth than other substrates, such as polyamide, polyimide, and Rogers 5880. The best impedance matching is achieved with the FR-4 substrate, to realize the desired operating bandwidth from 25.98 GHz to 40.18 GHz. However, at the higher operating frequencies, impedance bandwidth is noted slightly wider for the dielectric materials with low relative constant as Rogers 5800 $\varepsilon_r = 2.2$. As shown in Figure 10(b), the variation in gain results can be attributed to differences in the loss tangent values of each dielectric material. As the loss tangent increases, radiation performance deteriorates due to surface wave losses in the substrate material, particularly at higher frequencies.

The effects of various dielectric materials on the antenna's performance in terms of S_{11} and gain are summarized in Table 3. It can be concluded that FR-4 substrate is the optimal choice for designing the proposed antenna, as it ensures cost-effectiveness while achieving a wide operating bandwidth for $S_{11} < -10$ dB and maintaining good gain. In addition to offering a broad bandwidth and reliable gain, FR-4 substrate is readily available and has a lower fabrication cost than other more expensive substrate materials.

TABLE 3. Antenna's performance for various dielectric substrate.

Substrate	Operating bandwidth (GHz)	Gain (dB)
Polyamide	31.5–35.98 (4.48 GHz)	4.3–9.5
Polyimide	29.54–40.15 (10.61 GHz)	4.3–10
Rogers 5880	29.56–34.12 (4.56 GHz) 35.2–44 (8.8 GHz)	6–9.4
FR-4	25.98–40.18 (14.2 GHz)	4.8–7.87

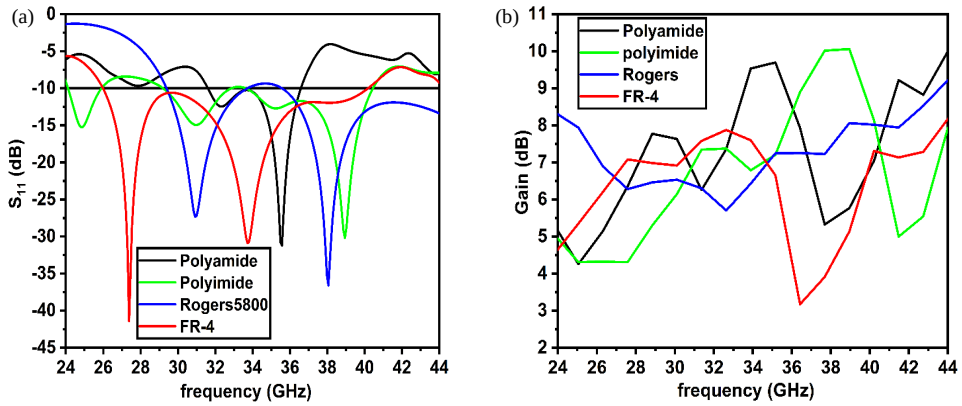

FIGURE 10. Impact of various substrate materials on antenna's performance, (a) S_{11}, (b) gain.

6. RESULTS AND DISCUSSION

To validate the simulated results and ensure design accuracy, the proposed broadband antenna was fabricated on a low-cost FR-4 substrate with a relative permittivity of 4.4, loss tangent of 0.02, and thickness of 0.8 mm, as depicted in Figure 11. The measured reflection coefficient results confirm that our final antenna is highly suitable for 5G applications in the millimeter-wave band, achieving a wide bandwidth of 14.20 GHz spanning from 25.98 GHz to 40.18 GHz.

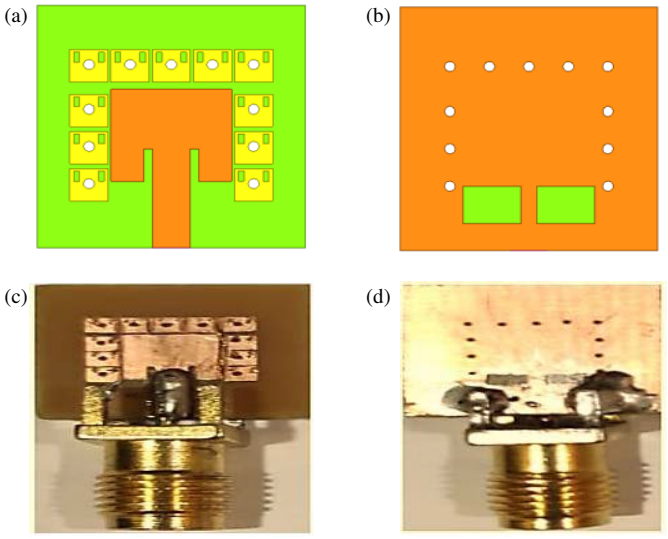

FIGURE 11. Design and fabricated prototype of the broadband antenna: (a) &(c) Top view, (b)&(d) bottom view.

Figure 12 illustrates both the simulated and measured reflection coefficients S_{11}. As observed from Figure 12, the measured reflection coefficient closely aligns with the simulated one. The measured results confirm that the antenna is well suited for the mm-wave band, offering a wide operating frequencies of 14.2 GHz, from 25.98 GHz to 40.18 GHz (which corresponds to a fractional bandwidth of 50.71%). The simulated results agree well with the measured ones. Figure 13 presents the radiation patterns in both the E-plane and H-plane for co-polarization, along with cross-polarization measurements at 28 GHz and 33 GHz. The antenna exhibits stable and symmetrical radiation patterns in both planes, with cross-polarization components approximately -30 dB below the main polarization. However, at higher frequencies, the radiation patterns degrade due to increased electrical thickness of the substrate and the presence of higher-order modes. Additionally, the cross-polarization component increases as the electrical thickness of the substrate and the relative permittivity of the substrate increase with frequency.

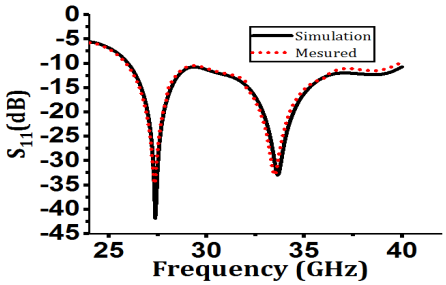

FIGURE 12. Simulated and measured results of reflection coefficients.

The peak gain and efficiency versus frequency of the proposed antenna are depicted in Figure 14. The antenna achieves a peak gain of 7.20 dB at 28 GHz, with a maximum gain of 7.87 dB at 32.67 GHz. Additionally, it demonstrates good radiation efficiency, ranging between 80% and 85% across the desired bandwidth. Figure 14(b) depicts the 3D gain pattern of the proposed antenna at 28 GHz, highlighting its strong radiation performance in terms of gain and efficiency. Figure 15 illustrates the Voltage Standing Wave Ratio (VSWR) of the proposed antenna, showing excellent impedance matching across the desired band. The VSWR remains below 2, reaching a minimum value of 1.005 at 28 GHz. The antenna maintains a wide bandwidth of 15 GHz, further demonstrating its robust performance.

7. COMPARISON STUDY

Table 4 summarizes the comparison study of the proposed antenna with existing works in the literature in terms of resonance frequency, substrate type, gain, reflection coefficient, impedance bandwidth (IBW), and directivity. From Table 2, it is evident that the proposed antenna generally outperforms

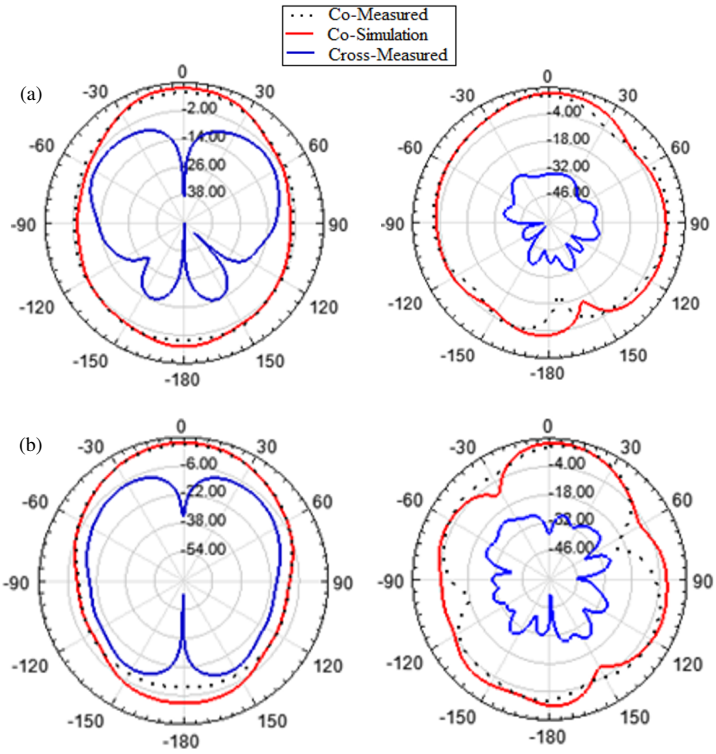

FIGURE 13. Radiation patterns of proposed antenna (a) 28 GHz, (b) 33 GHz.

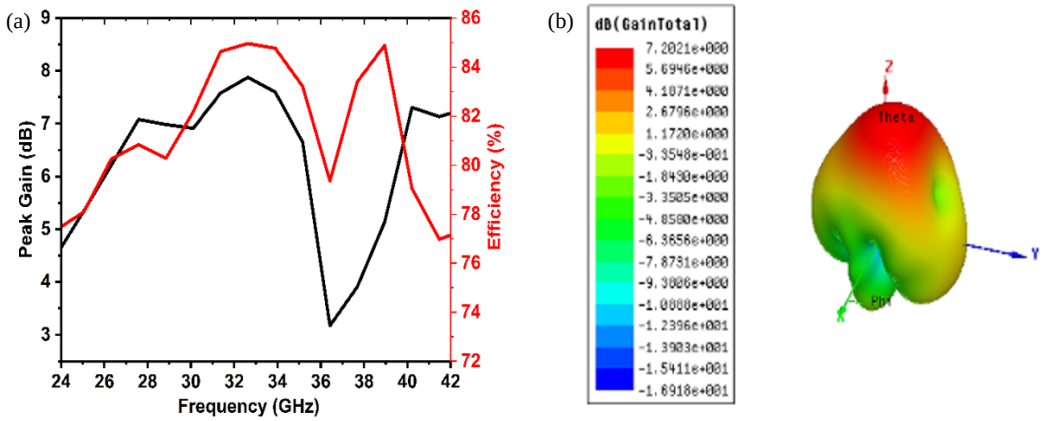

FIGURE 14. Simulated (a) peak gain and efficiency, (b) gain at 28 GHz of proposed antenna.

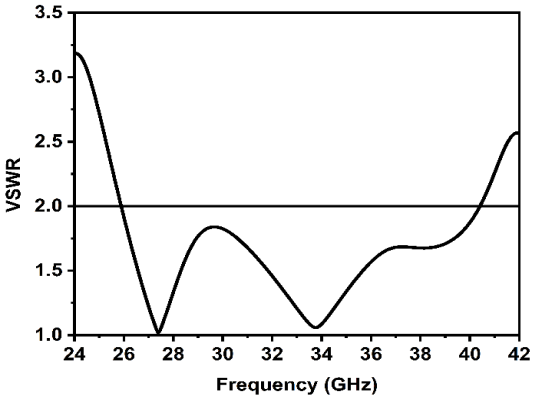

FIGURE 15. VSWR of proposed antenna.

other works. It achieves high gain and a wide bandwidth of 14.20 GHz. In contrast, antennas presented in [4, 5, 7], while being compact in size, suffer from lower bandwidth and gain than the proposed antenna. Other antenna structures in [4–9, 19–21] utilize high-cost Roger's substrate materials to achieve compact size and wide bandwidth. In contrast, the proposed antenna for 5G applications is designed using a low-cost FR-4 substrate. The use of parasitic patch mushroom structures and DGS improves the antenna's impedance bandwidth. The proposed antenna offers more than 75% wider bandwidth than recent literature, making it a promising choice for wideband applications.

TABLE 4. Performance comparisons.

Ref. Year	Fr (GHz)	Dielectric materials	Size (mm^3)	S_{11} (dB)	VSWR	IBW (GHz)	Gain (dB)
[7] 2022	mm-Wave	Rogers	$8.4 \times 6.2 \times 1.57$	-22.5	1.2	5.57	3.6
[8] 2022	mm-Wave	Rogers	$6 \times 6 \times 0.578$	-40	1.1	1.3	7.6
[9] 2022	mm-Wave	Rogers	$45 \times 40 \times 1.524$	-35.87	1.3	4	7.51
[10] 2022	mm-Wave	Rogers	$8.2 \times 14.5 \times 0.254$	-12.59	1.4	0.582	6.69
[11] 2022	mm-Wave	Rogers	$5.4 \times 7.6 \times 1.2$	-15	1.5	0.4	6.22
[12] 2022	mm-Wave	Rogers	$6.28 \times 7.235 \times 0.5$	-13.48	1.3	0.846	6.63
[22] 2024	mm-Wave	Rogers 5880	$6.15 \times 5.13 \times 0.8$	-35	N.A	39	5.2
[23] 2025	mm-Wave	Rogers 5880	$25 \times 33.5 \times 1.6$	-42	N.A	13.7	8.5
[24] 2024	mm-Wave	Rogers 5880	$10 \times 13 \times 1.6$	-30	N.A	4.5	6.5
This Work	**mm-Wave**	**FR-4**	$\mathbf{12 \times 13 \times 0.8}$	$\mathbf{-41.41}$	**1.005**	**14.20**	**7.20**

8. CONCLUSION

This paper presents a compact broadband rectangular antenna with high performance designed for the 5G mm-wave band, utilizing a parasitic mushroom patch and defect ground structure (DGS). The antenna's gain and bandwidth are enhanced through the use of a parasitic mushroom patch. Additionally, to extend the operating bandwidth to cover mm-wave frequencies for 5G applications, two rectangular DGSs are incorporated. The antenna prototype is fabricated and tested to validate the simulated results. It features a low profile of $12 \times 13 \times 0.8\,mm^3$. The proposed antenna achieves a gain ranging from 5 dB to 7.89 dB and maintains high efficiency between 80% and 85% across the entire bandwidth. Furthermore, the antenna demonstrates a wide operating bandwidth of 14.20 GHz, spanning from 25.98 GHz to 40.18 GHz. With these characteristics, the proposed antenna emerges as a strong candidate for 5G applications in the mm-wave band (28 GHz/38 GHz).

ACKNOWLEDGEMENT

The authors would like to thank Sidi Mohamed Ben Abdellah University of Morocco, Universiti Teknikal Malaysia Melaka (UTeM) and the Ministry of Higher Education (MOHE) of Malaysia for supporting this project.

REFERENCES

[1] Hussain, N., M.-J. Jeong, A. Abbas, T.-J. Kim, and N. Kim, "A metasurface-based low-profile wideband circularly polarized patch antenna for 5G millimeter-wave systems," *IEEE Access*, Vol. 8, 22 127–22 135, Jan. 2020.

[2] Elhabchi, M., M. N. Srifi, and R. Touahni, "A novel modified U-shaped microstrip antenna for super wide band (SWB) applications," *Analog Integrated Circuits and Signal Processing*, Vol. 102, 571–578, Jan. 2020.

[3] Kaeib, A. F., N. M. Shebani, and A. R. Zarek, "Design and analysis of a slotted microstrip antenna for 5G communication networks at 28 GHz," in *2019 19th International Conference on Sciences and Techniques of Automatic Control and Computer Engineering (STA)*, 648–653, Sousse, Tunisia, Mar. 2019.

[4] El Ansari, A., S. Das, T. Islam, S. Asha, N. E. A. E. Idrissi, and B. T. P. Madhav, "A high-gain directional 1×8 planar antenna array for 2.4 GHz RFID reader applications," *Journal of Circuits, Systems and Computers*, Vol. 33, No. 12, 2450219, 2024.

[5] El Ansari, A., S. Das, T. El-Arrouch, and N. E. A. E. Idrissi, "A hybrid coupler integrated 1×4 printed array antenna with broadband and high performance for beamforming RFID reader," in *2022 9th International Conference on Wireless Networks and Mobile Communications (WINCOM)*, 1–6, Rabat, Morocco, Oct. 2022.

[6] Ansari, A. E., T. Islam, S. V. R. Rao, A. Saravanan, S. Das, and N. E. A. E. Idrissi, "A broadband microstrip 1×8 magic-T power divider for ISM band array antenna applications," *J. Nano-Electron. Phys.*, Vol. 15, No. 3, 03003, 2023.

[7] Sohrabi, M., R. Hahnel, D. Plettemeier, S. Schindler, and H.-D. Wohlmuth, "5G mmWave dual-polarized stacked patch antenna," in *2021 51st European Microwave Conference (EuMC)*, 737–740, London, United Kingdom, Apr. 2022.

[8] Khan, M. M., H. M. A. Rahman, M. N. A. Shovon, W. Alhakami, M. Hadjouni, H. Elmannai, and S. Bourouis, "Design and analysis of a 5G wideband antenna for wireless body-centric network," *Wireless Communications and Mobile Computing*, Vol. 2022, No. 1, 1558791, Aug. 2022.

[9] Farag, H. A., A. E. Farahat, A. I. Bahnas, and K. F. A. Hussein, "Compact wideband single-side printed antenna for microwave and millimeter-wave wireless communications," *Progress In Electromagnetics Research C*, Vol. 126, 39–74, 2022.

[10] Madni, A., S. Zakir, R. M. H. Bilal, and W. T. Khan, "A compact inkjet-printed wide-band antenna for X/Ku/K/Ka-band and 5G applications," in *2022 IEEE International Symposium on Antennas and Propagation and USNC-URSI Radio Science Meeting (AP-S/URSI)*, 721–722, Denver, CO, USA, Jul. 2022.

[11] Umamaheswari, G. and A. Praveena, "A millimeter wave antenna for wireless body area network applications," in *2022 International Conference on Intelligent Innovations in Engineering and Technology (ICIIET)*, 118–123, Coimbatore, India, Sep. 2022.

[12] Elboushi, A. and A. M. Ameen, "Analysis and design of an oversized slotted patch antenna for 5G applications," *Int. J. Microw. Opt. Technol.*, Vol. 17, 10–15, 2022.

[13] Aghoutane, B., S. Das, M. El Ghzaoui, and B. T. P. Madhav, "A novel dual band high gain 4-port millimeter wave MIMO antenna array for 28/37 GHz 5G applications," *AEU-International Journal of Electronics and Communications*, Vol. 145, No. 16, 154071, 2022.

[14] Farahat, A. E. and K. F. A. Hussein, "Dual-band (28/38 GHz) wideband MIMO antenna for 5G mobile applications," *IEEE Access*, Vol. 10, 32 213–32 223, Mar. 2022.

[15] Hussain, M., E. M. Ali, S. M. R. Jarchavi, A. Zaidi, A. I. Najam, A. A. Alotaibi, A. Althobaiti, and S. S. M. Ghoneim, "Design and characterization of compact broadband antenna and its MIMO configuration for 28 GHz 5G applications," *Electronics*, Vol. 11, No. 4, 523, Feb. 2022.

[16] Ibrahim, A. A., H. Zahra, O. M. Dardeer, N. Hussain, S. M. Abbas, and M. A. Abdelghany, "Slotted antenna array with enhanced radiation characteristics for 5G 28 GHz communications," *Electronics*, Vol. 11, No. 17, 2664, Aug. 2022.

[17] Jayanthi, K., D. Kumutha, and M. Jeyabharathi, "Super compact FR-4 compatible 28 GHz antenna for 5G handheld devices," in *Distributed Computing and Optimization Techniques*, Vol. 903, 807–817, Sep. 2022.

[18] Park, J. S., J. H. Hong, and K. W. Kim, "Design of 24–40 GHz ultra-wideband circularly polarized monopole antenna with a defected ground plane," *Journal of Electromagnetic Engineering and Science*, Vol. 22, No. 3, 379–385, May 2022.

[19] Ullah, R., S. Ullah, R. Ullah, I. U. Din, B. Kamal, M. A. H. Khan, and L. Matekovits, "Wideband and high gain array antenna for 5G smart phone applications using frequency selective surface," *IEEE Access*, Vol. 10, 86 117–86 126, Aug. 2022.

[20] Askari, H., N. Hussain, M. A. Sufian, S. M. Lee, and N. Kim, "A wideband circularly polarized magnetoelectric dipole antenna for 5G millimeter-wave communications," *Sensors*, Vol. 22, No. 6, 2338, Mar. 2022.

[21] Ansari, A. E., V. Jayaprakasan, K. Duraisamy, S. Das, T. El-Arrouch, and N. E. A. E. Idrissi, "A wideband microstrip 1×2 array antenna fed by coupler for beam steering terahertz (THz) band applications," *J. Nano-Electron. Phys.*, Vol. 15, No. 3, 03028, 2023.

[22] Saha, D., I. M. Nawi, and M. A. Zakariya, "Super low profile 5G mmWave highly isolated MIMO antenna with 360° pattern diversity for smart city IoT and vehicular communication," *Results in Engineering*, Vol. 24, 103209, 2024.

[23] Rahman, M. A., S. S. Al-Bawri, S. S. Alharbi, W. M. Abdulkawi, N. M. Jizat, M. T. Islam, and A.-F. A. Sheta, "3D highly isolated 6-port tri-band MIMO antenna system with 360° coverage for 5G IoT applications based machine learning verification," *Scientific Reports*, Vol. 15, No. 1, 204, 2025.

[24] Rahman, M. A., S. S. Al-Bawri, W. M. Abdulkawi, and M. T. Islam, "Miniaturized tri-band integrated microwave and millimeter-wave MIMO antenna loaded with metamaterial for 5G IoT applications," *Results in Engineering*, Vol. 24, 103130, 2024.

[25] Al-Gburi, A. J. A., I. Ibrahim, Z. Zakaria, and A. D. Khaleel, "Bandwidth and gain enhancement of ultra-wideband monopole antenna using MEBG structure," *ARPN Journal of Engineering and Applied Sciences (JEAS)*, Vol. 14, No. 10, 3390–3393, 2019.

[26] Al-Gburi, A. J. A., "5G MIMO antenna: Compact design at 28/38 GHz with metamaterial and SAR analysis for mobile phones," *Przegląd Elektrotechniczny*, Vol. 100, No. 4, 171–174, 2024.

[27] Elabd, R. H. and A. J. A. Al-Gburi, "Super-compact 28/38 GHz 4-port MIMO antenna using metamaterial-inspired EBG structure with SAR analysis for 5G cellular devices," *Journal of Infrared, Millimeter, and Terahertz Waves*, Vol. 45, No. 1, 35–65, 2024.

[28] El Ansari, A., S. Khandare, K. Allabouche, N. E. A. E. Idrissi, Z. Zakaria, and A. J. A. Al-Gburi, "Conception and fabrication of a new steerable microstrip antenna for ISM band applications," *Progress In Electromagnetics Research Letters*, Vol. 126, 31–36, 2025.

[29] El Ansari, A., S. Das, N. E. A. E. Idrissi, T. El-Arrouch, and A. Bendali, "Slot incorporated high gain printed RFID reader array antenna for 2.4 GHz ISM band applications," in *E3S Web of Conferences*, Vol. 351, 01056, Istanbul, Turkey, May 2022.

[30] El Arrouch, T., N. E. A. E. Idrissi, and A. E. Ansari, "Microstrip patch antenna using a parasitic mushroom for 5G application at 28 GHz," in *2022 9th International Conference on Wireless Networks and Mobile Communications (WINCOM)*, 1–6, Rabat, Morocco, Oct. 2022.

[31] Ansari, A. E., S. Das, I. Tabakh, B. T. P. Madhav, A. Bendali, and N. E. A. E. Idrissi, "Design and realization of a broadband multi-beam 1×2 array antenna based on 2×2 Butler matrix for 2.45 GHz RFID reader applications," *Journal of Circuits, Systems and Computers*, Vol. 31, No. 17, 2250305, 2022.

[32] El Ansari, A., S. K. Khandare, N. E. A. E. Idrissi, A. Bendali, S. Das, F. Younis, H. K. Abduljaleel, and A. J. A. Al-Gburi, "Conception and realization of a wideband directional dual-beam phased MIMO array antenna with hybrid coupler for ISM band utilizations," *Progress In Electromagnetics Research M*, Vol. 132, 39–48, 2025.

[33] El Ansari, A., S. Das, T. Islam, V. Samudrala, N. F. Soliman, A. D. Algarni, and N. E. A. E. Idrissi, "A circularly polarized graphene based wideband 1×2 array antenna for terahertz spectrum applications," *Heliyon*, Vol. 10, No. 18, e37575, 2024.

[34] El Ansari, A., L. Kabouri, and E. Ahouzi, "Random attack on asymmetric cryptosystem based on phase-truncated Fourier transforms," in *2014 International Conference on Next Generation Networks and Services (NGNS)*, 65–68, Casablanca, Morocco, May 2014.